[Frontiers in Bioscience E5, 864-882, June 1, 2013]

Hybrid-drug design targeting *Pseudomonas aeruginosa* DHPS and DHFR

Premkumar Jayaraman[1], Kishore R Sakharkar[2] , Lim Chu Sing Daniel[1] , Mohammad Imran Siddiqi[3], Sarinder Kaur Dhillon[4], Meena K Sakharkar[5]

[1]Biomedical Engineering Research Centre, Nanyang Technological University, Singapore, [2]OmicsVista, Singapore, [3]Molecular and Structural Biology Division, Central Drug Research Institute, India, [4]Institute of Biological Sciences, Faculty of Science, University Malaya, Kuala Lumpur, Malaysia, [5]School of Life and Environmental Sciences, University of Tsukuba, Ibaraki, Japan

TABLE OF CONTENTS

1. ABSTRACT

In this study, we successfully present the dual-target design hypothesis to inhibit both dihydropteroate synthase (DHPS) and dihydrofolate reductase (DHFR) enzymes using a novel scheme that integrates our previous antibiotic-phytochemical interaction data, fragment combination and knowledge-based methods. Both the enzymes are well established antibacterial targets from folate biosynthesis pathway and their synergistic modulation by a single hybrid entity may have profound therapeutic benefits. Evaluation of the designed hybrid compounds based on their physico-chemical properties has indicated them as promising drug candidates with drug-like pharmacotherapeutic profiles. In addition, the stereo-electronic properties such as HOMO, LUMO and MEP maps calculated by quantum chemical methods gave a good correlation with the common pharmacophoric features required for dual-site interactions. Furthermore, docking and dynamics simulation studies reveal that the designed hybrid compounds have favorable binding affinity and stability in both pterin-binding site of DHPS and folate-binding site of DHFR by forming strong hydrogen bonds and hydrophobic interactions with key active-site residues. Looking forward this study could serve as a prospective lead in the process of new natural-product based hybrid-drugs development.

2. INTRODUCTION

Gram negative pathogens such as *Pseudomonas aeruginosa* have developed sophisticated resistance strategies through multiple mechanisms that have led to the selection of multi-drug resistant phenotypes, which have extremely limited the therapeutic options for Pseudomonas infections (1, 2). This opportunistic "ESKAPE" pathogen currently causes majority of the nosocomial and community-acquired infections and effectively "escapes" the effects of many commercially available antibacterial drugs, thereby joining the ranks of "superbugs" (1, 3). Despite ongoing efforts, only a very small number of novel anti-pseudomonal drugs are currently in late stage of pre-clinical or clinical development (4). Hence there is a pressing need to identify novel therapeutic strategies and more potent drugs to combat the constant evolution of resistance and circumvent the spread of multi-drug and pan-drug resistance development.

It is now widely recognized that, in contrast to 'one drug, one target, one disease', a single chemical entity able to target several nodes in a disease-causing network is considered to be highly beneficial for treating complex diseases (5, 6). Many specific lead generation strategies have been used earlier for the rational design of inhibitors with predefined multi-target profile, of which most

frequently reported is the framework combination strategy. In this approach, two separate pharmacophores that inhibit different targets are synthetically linked or merged into a single molecule (7, 8). The major complexity that is involved in the design of multiple ligands lies in balancing both drug-like physicochemical properties and desired multi-target profiles with unwanted off-target effects. However, if the starting compounds are small and the fragments are well integrated the framework combination strategy can be successful in generating multiple ligands with good oral bioavailability (9). Previously, several studies have proposed an alternative standard antibacterial therapy for broader empirical coverage through simultaneous administration of two drugs each with a separate action leading to a synergistic combination effect (10, 11). Though the use of combination therapy for serious infections is a recommended therapy in many hospitals, there are no direct evidences to support for its clinical effectiveness against *P. aeruginosa* infections and in addition there are many potential shortcomings using combination therapy of which more worrisome are drug toxicity, increased costs and increased risk of cross-infection creating more resistant organisms (12, 13). In comparison to the combination of drugs, multi-target conjugate ligands have greater predictable pharmacokinetic and pharmacodynamic relationships, increased penetration capacity due to the additional pharmacophore, lower toxicity and thus delay the onset and overcome the existing bacterial resistance mechanisms (7). Recently, the hybrid antibiotics approach in targeting multiple enzymes has been quite successful, such as trimethoprim (benzyl pyrimidine) linked fluroquinolone (BP-4Q-002) hybrid compounds (14), aminoglycoside-fluroquinolone (15) and peptide-aminoglycosides hybrids (16) have been shown to be potent antimicrobial agents against both gram negative and gram positive bacteria. In addition, three hybrid compounds TD-1792, MCB-3837 and CBR-2092 currently in human clinical trials are reported to have significantly higher activity against multi-drug resistant strains in comparison to both the drugs alone and in combination (7). Therefore from the recent progress, design and development of multi-target hybrid compounds emerges clearly as a promising strategy for fresh research avenues.

On the basis of target relationship (17), therapeutic effect by multi-target drugs can be achieved in several categories, (i) modulation of one target facilitating action at the second target (e.g., inhibition of efflux pumps or by altering compound metabolism), (ii) binding multiple sites on the same target leading to a combination effect (e.g., prokaryotic ribosomes), (iii) by targeting separate molecular targets that can reside in the same or separate pathway within an individual cell or in separate tissues leading to a combination effect (co-trimoxazole, folic acid biosynthesis pathway). In the third category, co-trimoxazole a cocktail of two drugs (trimethoprim and sulfamethoxazole), trimethoprim (TMP, diaminopyrimidine antibiotic) inhibits dihydrofolate reductase (DHFR) enzyme which catalyzes the NADPH-dependent reduction of dihydrofolic acid to tetrahydrofolic acid and sulfamethoxazole (SMX, sulfonamide antibiotic) competitively inhibits the *p*-aminobenzoic acid (*p*ABA) incorporation into bacterial dihydropteroic acid in dihydropteroate synthase (DHPS) enzyme and are synergistic in combination as it causes sequential blockade of two consecutive steps in the folate biosynthesis pathway (18). However in addition to serious side effects, numerous antifolate resistance mechanisms have developed rapidly among all major pathogenic microorganisms limiting the use of sulfonamides, trimethoprim and even their combination (19). In the case of *P. aeruginosa*, trimethoprim and sulfonamides have minimum inhibitory concentration (MIC) usually in the resistance range due to low outer membrane permeability, poor affinity and characteristic intrinsic resistance by efflux pumps (20). The *p*ABA/sulfonamide binding site is situated in the flexible loop regions at the C-terminal in DHPS, that is open to range of mutations that confer sulfonamide resistance (21). In contrast, the pterin binding pocket is located deep inside the active site cavity which is highly conserved in several common pathogenic bacteria and targeting this distinct site is considered to be highly advantageous as it can bypass the sulfonamide resistance sites (22). Recently, Bennett *et al.* (23) reported an inhibitor (MANIC compound) that binds to both the pterin site of DHPS and folate binding site of DHFR inhibiting both the enzymes. The use of this inhibitor as a fragment to build compounds that are more potent against both the enzymes was also suggested (23). On the other hand, a study using epigallocatechin gallate (EGCG) a catechin found in green tea, Navarro-Martinez and colleagues showed that EGCG has antifolate activity similar to that of TMP and is synergistic in combination with SMX. The use of EGCG as an alternative to TMP in combination with SMX for the treatment of *S. maltophilia* infections was also reported (24). Similarly, in our recent work using drug-phytochemical combination assays we proposed that phytochemicals (protocatechuic acid, gallic acid – phenolic acids), which are fragments of EGCG and show antifolate activity by binding to DHFR and are also synergistic in combination with sulfonamide antibiotics (sulfamethoxazole and sulfadiazine) (25-27). One limitation in this study was the higher minimum inhibitory concentration (MIC) for phytochemicals in comparison to that of the antibiotics used. Supporting this several reports have claimed that dietary phytochemicals are less potent due to their higher MIC's, have lesser stability and selectivity, have adverse phytochemical-antibiotic interactions and lesser bioavailability in comparison to the compounds from microbial origin (antibiotics) (28, 29). Traditionally, plants have continued to be significant natural source of several drug leads as they have limitless abilities to synthesize highly diverse secondary metabolites possessing weak to very strong antimicrobial activities against various organisms (30, 31). These phytochemicals can be described as "privileged structures" because of their diverse chemical scaffolds which are naturally selected by evolutionary pressures that have the ability to interact with wide variety of proteins and other biological targets for specific reasons (32). Notably, the effectiveness of natural products in the drug discovery and development process is evident as more than 75% of the drugs for infectious diseases are natural compounds and their derivatives (33). Moreover, the natural products are amenable to further improvement to facilitate efficacy and selectivity for the

target or to achieve optimal pharmacokinetic and pharmacodynamic properties (34). _ENREF_4Interestingly, it has been proposed that phytochemicals can be converted to pharmacologically acceptable antimicrobial agents by optimization through structural modifications (35).

In view of this using fragment combination approach, here we describe a novel hypothesis that is focused on the rational design of novel hybrid compounds based on the modification of phytochemicals by coupling two molecular entities (structural analogue of MANIC compound fragment and phytochemicals) using a non-cleavable linker for dual inhibition of DHPS and DHFR enzymes in the folate biosynthesis pathway. Further on, we also successfully demonstrate the dual-action hybrid compound hypothesis using various integrated computer-aided molecular modeling methodologies and knowledge-based methods. The in silico based methods such as molecular docking, combined molecular docking and common pharmacophore identification and fragment combination have earlier been shown to be successful in the design and discovery of multi-target compounds directed at selective multiple targets (36). The knowledge based methods which employs the text mining of scientific literature are commonly used to establish link and create novel hypothesis by combining information from numerous papers (37). The knowledge based approach used in this study integrates both receptor based information and common pharmacophoric features required for the dual target inhibition. We also investigated the proposed hybrid compounds drug-like pharmacotherapeutic profiles using various physico-chemical properties prediction mechanism and verified the derived common pharmacophoric features using stereo-electronic properties calculated by quantum chemical methods. To the best of our knowledge, this study is the first to successfully combine knowledge from the scientific literature with previous drug combination data and fragment combination approach towards the identification of novel dual-action hybrid compounds that can strongly bind at the active site cavities of both DHPS and DHFR enzymes. This study also forms a base for multi-target drug discovery and reveals the enhancement of phytochemicals through hybrid design framework for the discovery of new and potent drugs in the treatment of complex diseases.

3. METHODS

3.1. Ligand dataset preparation and properties prediction

The primary 3D chemical structures of the designed hybrid compounds were generated through shell script in Open Babel (http://openbabel.sourceforge.net/) using the SMILES notation (.smi) as the input and the output files were saved in SDF file format (38). The SMILES (.smi) formats were prepared using Marvin Sketch (Chemaxon), advanced chemical drawing software. The generated 3D structures were subjected to conformational search calculations in gas phase using Merck Molecular Force Field (MMFF) method in SPARTAN' 10 program (39). The minimum energy conformation was chosen for geometry optimization using the Austin model 1 (AM1) semi-empirical algorithm. The optimized structures were re-optimized using the density functional theory (DFT), hybrid B3LYP/6-31G** basis-set functional (40). The stereo-electronic properties such as HOMO, LUMO energies, band gap (HOMO - LUMO), molecular electrostatic potential, dipole moment and polarizability, physico-chemical properties (molecular volume, polar surface area) and absolute energies were calculated from single-point energy calculations on the complete geometry optimized structures of the designed compounds using B3LYP/6-31G** basis-set. In addition, absorption (%) was also calculated by using the following equation: %ABS = 109 – (0.354 x PSA) based on the computed PSA values (41).

To obtain additional insights on the physico-chemical properties (molecular weight, cLogP, solubility, polar surface area, number of hydrogen bond donors and acceptors, number of rotatable bonds, drug-likeness, overall drug-score) and the toxicity risks (mutagenicity, tumorigenicity, irritating, reproductive effects) of the designed hybrid compounds, commercially available DHPS inhibitors (sulfamethoxazole and sulfadiazine), DHFR inhibitors (methotrexate and trimethoprim), MANIC compound and phytochemicals (epigallocatechin gallate, *p*-hydroxy benzoic acid, protocatechuic acid, vanillic acid, gallic acid, syringic acid and eudesmic acid) used in this study were predicted using online OSIRIS (http://www.organic-chemistry.org/prog/peo/) and Molinspiration (http://www.molinspiration.com/cgi-bin/properties) property prediction toolkits. The 2D structures of the compounds were drawn on the Actelion and molinspiration property explorer and the drug relevant properties were predicted accordingly. The toxicity risk assessment indicates potential toxicity risks in the drawn structure concerning the risk category specified and the process relies on the pre-computed set of structural fragment that give toxicity alerts if they are encountered in the drawn 2D structures. Properties with high risks of undesired effects like mutagenicity or a poor intestinal absorption are shown as negative sign, whereas positive sign indicates drug conform behavior.

3.2. Target structure preparation

The protein sequence of the target enzymes *Pseudomonas aeruginosa* (PA01, Tax ID - 208964) dihydropteroate synthase (folP, Locus ID – PA4750) and dihydrofolate reductase (folA, Locus ID – PA0350) were retrieved from Pseudomonas genome database (http://www.pseudomonas.com/). Homologous sequences of *P. aeruginosa* DHPS and DHFR were obtained from NCBI by BLASTP search against Protein Data Bank (PDB) and SWISS-MODEL template selection tool using *P. aeruginosa* DHPS and DHFR as query sequences. Based on the template selection analysis, *E. coli* DHPS (PDB code: 1AJ0, 2.0 Å) and *E. coli* DHFR (PDB code: 1RX3, 2.2 Å) were selected as suitable templates with identity scores of 61% and 45%, respectively. The alignment of *P. aeruginosa* DHPS and DHFR protein sequences and template structures - *E. coli* DHPS (1AJ0) and DHFR (1RX3) protein sequences,

were performed using CLUSTALW2 (http://www.ebi.ac.uk/Tools/clustalw2/index.html). The 3D model building of DHPS and DHFR was carried out using two automated modeling programs: SWISS-MODEL (42) and MODELLER 9v7 (43) using templates 1AJ0 and 1RX3 retrieved from the PDB (http://www.rcsb.org/pdb/). The generated homolog models were submitted to WHAT IF server (http://swift.cmbi.ru.nl/servers/html/index.html) to model missing side chains and remove atomic clashes (bumps) (44). The RMSD values between the predicted *P. aeruginosa* DHPS and DHFR models obtained from both SWISS-MODEL and MODELLER and *E. coli* templates were calculated using the SUPERPOSE (45) web server (http://wishart.biology.ualberta.ca/SuperPose/). Out of all the models estimated, the SWISS-MODEL constructed models resulted in low RMSD values of ~ 0.5 Å and were thus selected for further investigations. The models were then subjected to validate the quality using SWISS-MODEL structure assessment tool (42) with PROCHECK, WHATCHECK, QMEAN and ANOLEA. The overall quality score displayed in the context of all known protein structures were also calculated using the web-based PROSA analysis (46) (https://prosa.services.came.sbg.ac.at/prosa). Finally, Verify-3D (47) was used to measure the compatibility of the obtained model with its amino acid sequence.

3.3. Molecular docking

In order to study the binding modes of the designed hybrid compounds in the active site cavities of the modeled P. aeruginosa DHPS and DHFR enzymes, docking experiments were carried out using MolDock (Molegro virtual docker) docking engine, which is based on a new heuristic search algorithm that combines differential evolution with a cavity prediction algorithm (48). The homology models generated were maintained throughout the docking experiments. The ligands from the crystal structure of *E. coli* DHPS and DHFR were transferred into the workspace keeping the orientation as a control and were kept as reference ligand. The ligand binding modes were assumed to be similar in both target and template structure. The complete geometry optimized structures of the hybrid compounds and the generated protein homologs were also transferred and hydrogens were added to both ligands and protein molecules using the preparation wizard in the Molegro workspace. During import of the 3D structures of the ligands, charges, bond orders were assigned, the torsional angle of the 3D structures were also determined and all acyclic single bonds were set as flexible. Binding sites in the electrostatic surface of the protein were identified using the grid based cavity prediction algorithm. A total of five cavities were detected and the prepositioned reference ligand in the active site cavity was identified and the docking was constrained to the predicted active site cavity. MolDock [Grid] scoring function using template docking with default values: -500 overall strength and 0.4Å energy grid resolution was used to evaluate the energy between the ligand and the target enzyme. Grid resolution, number of runs, population size, maximum iterations, pose generation energy threshold, simplex evolution max steps and neighbor distance factor were set as 0.30Å, 20, 50, 1500, 100, 1.00 for each run, respectively using the MolDock SE algorithm. Multiple poses were returned for each run with the RMSD threshold set to 1.00Å. The pose with the highest Rerank and Moldock score was retained in the workspace for detailed evaluation of the binding mode at the active site cavity. Along with both MolDock and reranking scores, we also predicted binding affinities using a calibrated model that is included in the MVD. The binding affinity model was trained using a data set of more than 200 structurally diverse complexes from PDB with known binding affinities (49). Thus, in our docking experiments we used this recommended strategy of ranking the docking results by their rerank scores and subsequently the binding affinity measure to get high ranked poses. The validation of the docking protocol was carried out by re-docking the imported reference ligands from their respective experimental PDB structures in the predicted active site cavity of the models using the RMSD measure. The RMSD values for the re-docked methotrexate (MTX) and NADP in the model (*P. aeruginosa* DHFR) active site were 0.3968Å and 0.5794Å, respectively and DHP (6-hydroxymethyl-7,8-dihydropterin) in the model (*P. aeruginosa* DHPS) was 0.3934Å. Furthermore, the binding conformations of ligands in the enzyme active site cavity were analyzed by visualizing the H-bond and electrostatic interactions formed between the ligands and the active site residues.

3.4. Molecular dynamics simulations

YASARA dynamics package version 10 (50) was used to perform the molecular dynamics simulations analysis for the top ranked docked inhibitor in both the enzymes, their corresponding ligand bound enzymes and unbound enzymes using the AMBER03 force field. A periodic simulation cell of at least 20 Å larger than the protein was employed with TIP3 water around the *P. aeruginosa* enzyme complexes (I – DHPS, IV – DHFR, II – DHPPP-DHPS, V – MTX-NADP-DHFR) and top ranked hybrid compound-bound enzyme complexes (III – HD_EA-DHPS and VI – HD_EA-NADP-DHFR) were energy minimized to correct the covalent geometry and to remove bumps. The AMBER03 force field was used with Van der Waals pairs cut-off distance 7.86Å and long range statistics algorithm calculated using the Particle Mesh Ewald (PME) method (51). The Na^+ and Cl^- counter ions were added at the most favorable positions to neutralize the ion strength in the cell. The density of the water filled in the simulation cell was 0.997g/l and the pressure was controlled by rescaling the simulation box dimensions to maintain the water density. The pKa values were predicted using the empirical pKa prediction equation that is approximated as a function of electrostatic potential, hydrogen bonds and accessible surface area by Ewald summation implemented in YASARA (52). A short MD was run on the solvent only and the entire system was energy minimized by steepest descent minimization to remove conformational stress and subsequently followed by simulated annealing minimization using a time step of 2fs and atom velocities scaled down by 0.9 every 10^{th} step until convergence (energy improved by less than 0.1% during 200 steps). The MD simulation was then initiated, with temperature fixed at 298K and multiple time-steps were set for intramolecular and intermolecular forces at 1.33 and 4 fs respectively.

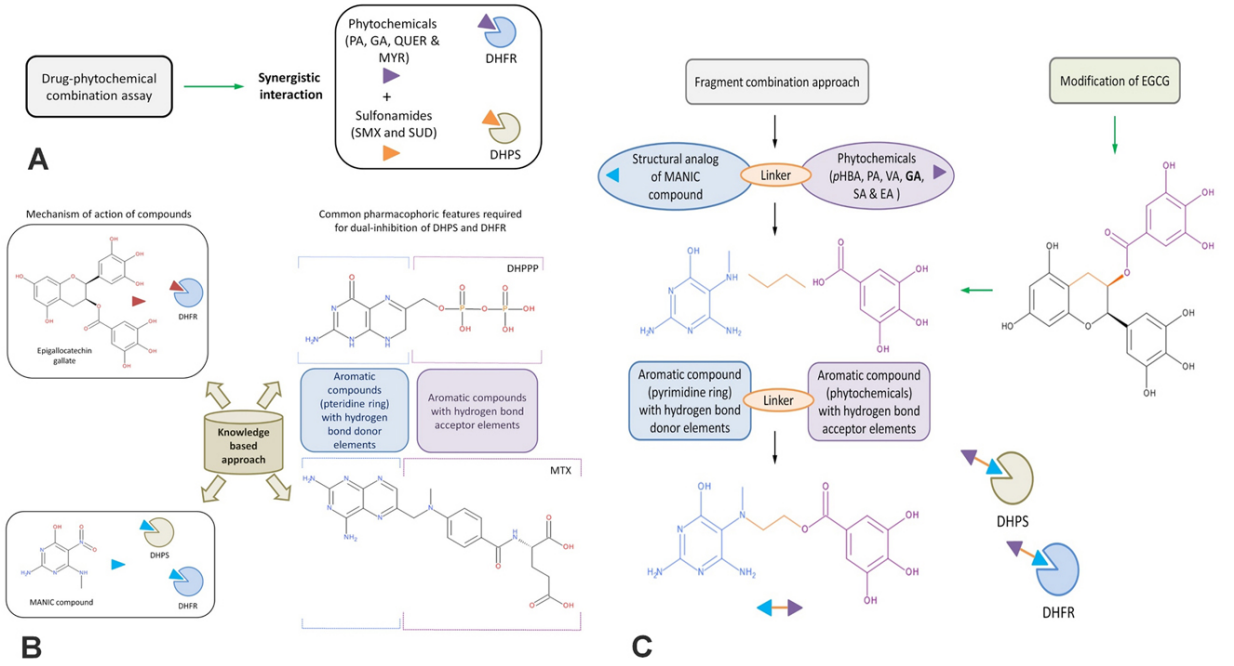

Figure 1. How we identified the targets? - Hypothesis and design of dual action compounds. (A) Drug-phytochemical interactions identified using combination assays. (i) The green arrow signifies synergistic interaction of phytochemicals (protocatechuic acid (PA), gallic acid (GA), quercetin (QUER) and myricetin (MYR), represented as violet arrow head) in combination with sulfonamide antibiotics (sulfamethoxazole (SMX) and sulfadiazine (SUD), represented as orange arrow head). The sulfonamides block the dihydropteroate synthase (DHPS) enzyme, while the phytochemicals target the subsequent enzyme dihydrofolate reductase (DHFR) in the folate biosynthesis pathway leading to a synergistic effect; (B) Knowledge based approach was used to establish relationship between therapeutic targets (DHPS and DHFR) identified based on our previous drug-phytochemical interaction network. (i) Mechanism of action of epigallocatechin gallate (plant flavonoid, red arrow head) targeting DHFR and previously reported MANIC compound that binds to both DHPS & DHFR enzymes, illustration of the ability of these compounds to bind to these enzymes. (ii) Common pharmacophoric features derived for dual-inhibition of DHPS and DHFR enzymes from previously reported individual pharmacophore models and known pterin/pteridine based inhibitors; (C) Schematic illustration of the fragment combination method used to derive the hybrid compounds (structural analog of MANIC compound (blue arrow head) linked with phytochemicals (violet arrow head) using non-cleavable linker (orange line) that can simultaneously bind to both DHPS & DHFR enzymes.

Each complex was subjected to 3000ps of molecular dynamics simulations and snapshots were saved every 1ps for data analysis. The trajectories of the molecular dynamics simulations were analyzed for the equilibrium stability by measuring the root mean square deviations (RMSD) of the complexes and the root mean square fluctuation (RMSF) of residues around the ligand-binding active sites.

4. RESULTS AND DISCUSSION

4.1. Dual target design hypothesis

Recently, we proposed that phytochemicals (protocatechuic acid, gallic acid, quercetin and myricetin) which are fragments and catechin analogs/derivatives of EGCG, bind to DHFR and are synergistic in combination with sulfonamide antibiotics (sulfamethoxazole and sulfadiazine) (25-27), schematically represented in Figure 1a. In another interesting study, a small compound named MANIC was postulated to bind in the pterin ring pocket at the dihydropteroate synthase (DHPS) active site competing with the dihydropterin pyrophosphate (DHPPP) substrate and also to the subsequent enzyme dihydrofolate reductase (DHFR) interfering with the dihydrofolate (DHF) substrate in the folate biosynthesis pathway (23), shown in Figure 1b.

Based on these data, as a first step in our dual-target design hypothesis using knowledge-based methods we identified important interactions required for the inhibition of both DHPS and DHFR based on their individual pharmacophore models and known pterin/pteridine based inhibitors (22, 53). Combining these models we derived a common pharmacophoric model for dual inhibition of both the enzymes (1) an aromatic element (pteridine type moiety) with hydrogen-bond donor elements mapping the pterin moieties of dihydropterin pyrophosphate in DHPS and dihydrofolate in DHFR, (2) *p*ABA binding site in DHPS and *p*-aminobenzoate linker and glutamate tail region of folate, maps for aromatic/hydrophobic element with hydrogen-bond acceptor elements (22, 53).

We embarked on using the structural analog of MANIC compound (2,6-diamino-5-

Table 1. Calculated toxicity risks, molecular properties, drug-likeness and overall drug-score of the designed hybrid compounds and commercially available DHPS and DHFR inhibitors investigated

Compounds	Toxicity risks prediction				Molecular properties								
	MUT[1]	TUM[2]	IRR[3]	REP[4]	MW[5]	cLP[6]	S[7]	nON[8]	nOHNH[9]	nViolations	nRotb[10]	D_L[11]	D_S[12]
HD_*p*HBA	+	+	+	+	319	1.15	-2.9	9	6	1	6	5.1	0.88
HD_PA	+	+	+	+	335	0.85	-2.61	10	7	1	6	5.02	0.89
HD_VA	+	+	+	+	349	1.04	-2.92	10	6	1	7	4.62	0.87
HD_GA	+	+	+	+	351	0.55	-2.31	11	8	2	6	5.29	0.89
HD_SA	+	+	+	+	379	0.94	-2.94	11	6	2	8	6.27	0.85
HD_EA	+	+	+	+	393	1.13	-3.25	11	5	1	9	9.0	0.82
Sulfamethoxazole	+	-	+	+	253	0.7	-3.02	6	3	0	3	3.31	0.54
Sulfadiazine	+	+	+	-	250	0.41	-2.29	6	3	0	3	4.09	0.56
Methotrexate	+	-	+	+	454	-0.69	-3.77	13	7	2	9	-7.09	0.22
Trimethoprim	+	+	+	+	290	1.23	-3.32	7	4	0	5	4.95	0.87
MANIC	+	+	+	+	185	0.03	-2.41	8	4	0	2	-0.88	0.61

[1]MUT: mutagenicity, [2]TUM: tumorigenicity, [3]IRR: irritating effects, [4]REP: reproductive effects, [5]MW: molecular weight, [6]cLP: cLogP, [7]S: Solubility, [8]nON: number of hydrogen bond acceptors (O and N groups), [9]nOHNH: number of hydrogen bond donors (OH and NH groups), [10]nRotb: number of rotatable bonds, [11]D_L: druglikeness, [12]D_S: drug score, + : Toxic free, - : Toxic behavior.

(methylamino)pyrimidin-4-ol), to satisfy the common pharmacophoric feature **(1)** linked with a non-cleavable linking group (hydrophobic element) to another aromatic element with hydrogen bond acceptor moieties **(2)**, the phytochemicals (protocatechuic acid (PA) & gallic acid (GA)) used in our previous drug combination assay and their structural analogues (*p*-hydroxy benzoic acid (*p*HBA), vanillic acid (VA), syringic acid (SA) & eudesmic acid (EA)). This demonstration of the semi-synthetic modification of the phytochemicals is based on the active natural compound EGCG skeleton which is a well-known DHFR inhibitor and this molecular tinkering leads to the identification of entirely novel hybrid compounds, selective against both DHPS and DHFR enzymes, schematically represented in Figure 1c.

The most intriguing aspect in our hybrid design strategy is the approach for chemical modification of natural product-based inhibitors of DHFR through structural combination with another fragment (common DHPS and DHFR inhibitor) which may help improve the properties and also bypass the mechanism of resistance coupled with the integration of dual-target specificity. It is also significant that the designed dual ligands are highly desirable as it will be much difficult for a pathogen to develop resistance when an inhibitor has activity against two different enzymes involved in folate biosynthesis and this approach would be potent and beneficial armor for the therapeutic intervention of robust pathogens.

4.2. In silico calculations of physico-chemical, drug-likeness and toxicity risks analysis

We investigated relevant toxicity risks, physico-chemical properties, drug-likeness and bioavailability of compounds using various *in silico* based prediction tools.

The predicted toxicity risks shown in (Table 1) indicate that all the hybrid compounds are non-mutagenic, non-tumorigenic, non-irritating and non-reproductive and are comparable to standard traded drugs. For comparison, we evaluated the toxicity risks of MANIC compound, commercially available DHPS (sulfamethoxazole & sulfadiazine), DHFR inhibitors (methotrexate & trimethoprim) of which trimethoprim and MANIC compound showed toxic free effects while, methotrexate showed risks concerning reproductive and tumorigenic effects, sulfamethoxazole showed tumorigenic risk effects and sulfadiazine was found to be associated with reproductive toxicity alert. Also, the predicted toxicity risks for phytochemicals (EGCG, *p*HBA, PA, VA, GA, SA & EA) in Table 2 showed mutagenic effects for PA, VA, GA & SA and also an additional reproductive effect for GA, while EGCG, *p*HBA and EA showed toxic free behavior. Overall, the designed natural-product based semi-synthetic hybrid structures (HD_*p*HBA, HD_PA, HD_VA, HD_GA, HD_SA and HD_EA) in Figure 2 showed non-toxic behavior with highly desirable physico-chemical parameters disclosing their potential as promising agents for antimicrobial therapy.

The physico-chemical properties such as, molecular weight of the proposed hybrid compounds is below 400 (Table 1) and thus they are more likely to have higher absorption. The clogP value is the logarithm of its partition coefficient between n-octanol and water, measuring the compound's hydrophilicity (54). The estimated clogP values for the proposed compounds are less than 5.0 indicating high lipophilicities, higher absorption and permeation. Aqueous solubility (log S) measures significantly affect the drug absorption/distribution characteristics and the estimated log S value is a unit stripped logarithm of the solubility (moles/liter). It is suggested that more than 80% of the drugs in the market have log S value greater than -4 (http://www.organic-chemistry.org/prog/peo/). The solubility measures for the proposed compounds in (Table 1) are in the expected range of -2.31 to -3.25 and are comparable to that of the standard commercially available drugs. The number of Lipinski's RO5 violations is one each for the designed hybrid compounds HD_*p*HBA, HD_PA, HD_VA, HD_EA, which are within the range sets defined for oral bioavailability and two for HD_GA and HD_SA. The number of rotatable bonds and polar surface area are now widely used filter for drug-likeness and those compounds which meet only the two criteria of (1) $\leq$ 10 rotatable bond counts and (2) polar surface area (PSA) $\leq$ 140 Å^2 (or $\leq$ 12 H-bond donors and acceptors) will have increased oral bioavailability in the rat (55). The calculated

Table 2. Calculated toxicity risks, molecular properties, drug-likeness and overall drug-score of the phytochemicals and MANIC compound investigated

Compounds	Toxicity risks prediction				Molecular properties								
	MUT[1]	TUM[2]	IRR[3]	REP[4]	MW[5]	cLP[6]	S[7]	nON[8]	nOHNH[9]	nViolations	nRotb[10]	D_L[11]	D_S[12]
Epigallocatechin gallate	+	+	+	+	458	2.65	-2.16	11	8	2	4	1.58	0.69
p-hydroxy benzoic acid (*p*HBA)	+	+	+	+	138	1.2	-1.33	3	2	0	1	-1.5	0.57
Protocatechuic acid (PA)	-	+	+	+	154	0.9	-1.04	4	3	0	1	-0.12	0.43
Vanillic acid (VA)	-	+	+	+	168	1.1	-1.35	4	2	0	2	-1.31	0.35
Gallic acid (GA)	-	+	+	-	170	0.6	-0.74	5	4	0	1	0.12	0.27
Syringic acid (SA)	-	+	+	+	198	0.99	-1.37	5	2	0	3	1.99	0.54
Eudesmic acid (EA)	+	+	+	+	212	1.19	-1.68	5	1	0	4	5.61	0.96

[1]MUT: mutagenicity, [2]TUM: tumorigenicity, [3]IRR: irritating effects, [4]REP: reproductive effects, [5]MW: molecular weight, [6]cLP: cLogP, [7]S: Solubility, [8]nON: number of hydrogen bond acceptors (O and N groups), [9]nOHNH: number of hydrogen bond donors (OH and NH groups), [10]nRotb: number of rotatable bonds, [11]D_L: druglikeness, [12]D_S: drug score, + : Toxic free, - : Toxic behavior.

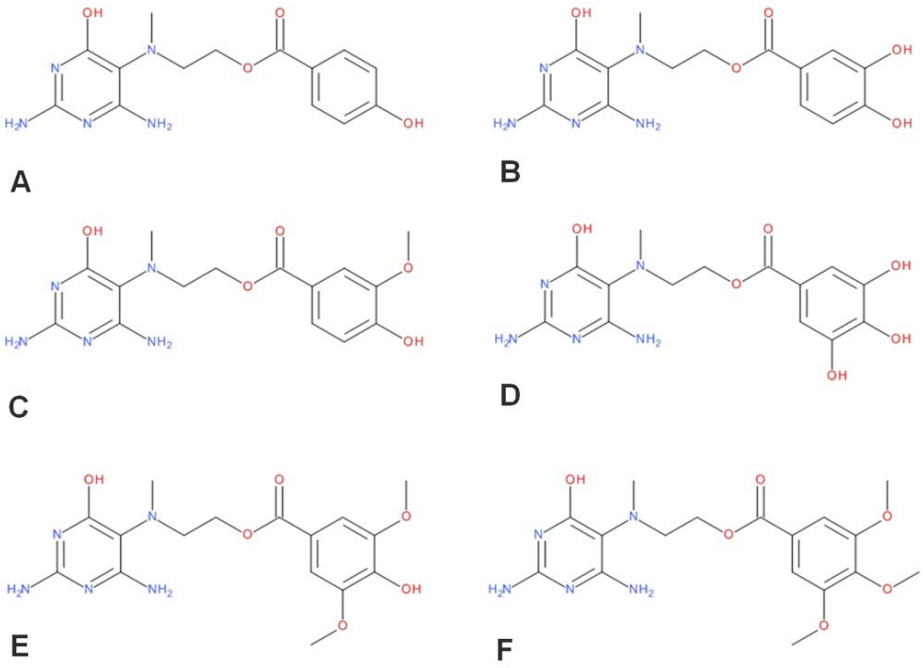

Figure 2. Structures of the designed hybrid compounds. (A) HD_*p*HBA; (B) HD_PA; (C) HD_VA; (D) HD_GA; (E) HD_SA; (F) HD_EA

rotatable bond counts (Table 1) of the proposed compounds are ≤ 4 and PSA are within the range for compounds HD_*p*HBA, HD_VA, HD_SA, HD_EA and just above for compounds HD_PA and HD_GA (Table 3). On the other hand using PSA, we calculated the percentage of absorption (%ABS) according to the equation %ABS = 109 – (0.354 x PSA), as reported by Zhao *et al.* (41), the calculated absorption percentage are in the range of 52-66% for all the proposed compounds (Table 3). Drug-likeness scores are calculated by summing up score values, partially based on topological descriptors, fingerprints of MDL structure keys including properties such as clogP and molecular weight are estimated to be in the positive range for 80% of the traded drugs (http://www.organic-chemistry.org/prog/peo/). The drug-likeness scores for the proposed compounds are positive (Table 1) indicating that the molecules predominantly contain fragments which are frequently present in commercial drugs and hence have the possibility of being "drug-like". Finally, the overall drug score (Table 1) combining drug-likeness, cLogP, logS, molecular weight and toxicity risks describe the potential to qualify for a drug in 0 to 1 scale (http://www.organic-chemistry.org/prog/peo/). Compared to the overall drug scores of the phytochemicals and MANIC compound alone, the conjugated hybrid compounds scores were in the range of 0.82 – 0.89 (Table 1) indicating the proposed compounds potential to qualify as suitable drug candidates.

Table 3. Absolute energies, stereo-electronic and molecular properties calculated at B3LYP/6-31G** basis-set levels and percentage of absorption of the designed hybrid compounds.

Compounds	Energy[1] (in hartress)	Energy(aq)[2] (in hartress)	Energy(S)[3] (KJ/mol)	%ABS[4]	Volume (Å^3)	PSA[5] (Å^2)	E_{HOMO} (eV)	E_{LUMO} (eV)	Band gap (ΔE)[6] (eV)	Dipole moment (debye)	Polarizability
HD_*p*HBA	-1118.42	-1118.42	-108.49	66	304.85	122.82	-5.84	-1.02	-4.82	5.65	64.96
HD_PA	-1193.63	-1193.68	-125.56	59	312.00	142.22	-5.85	-1.06	-4.79	4.46	65.55
HD_VA	-1232.94	-1232.98	-113.85	63	333.14	130.08	-5.84	-0.97	-4.87	5.00	67.25
HD_GA	-1268.85	-1268.9	-133.96	52	319.12	160.75	-5.89	-1.03	-4.86	3.51	66.11
HD_SA	-1347.45	-1347.5	-106.66	61	360.14	136.29	-5.87	-0.94	-4.93	4.03	69.42
HD_EA	-1386.75	-1386.79	-100.36	65	380.62	125.11	-5.88	-0.99	-4.89	3.10	71.09

[1]Energy: Total energy in vacuo, [2]Energy (aq): Total energy in aqueous medium, [3]Energy(S): aqueous salvation energy, [4]%ABS: Absorption, [5]PSA: polar surface area, [6]ΔE: $\Delta E_{HOMO-LUMO}$.

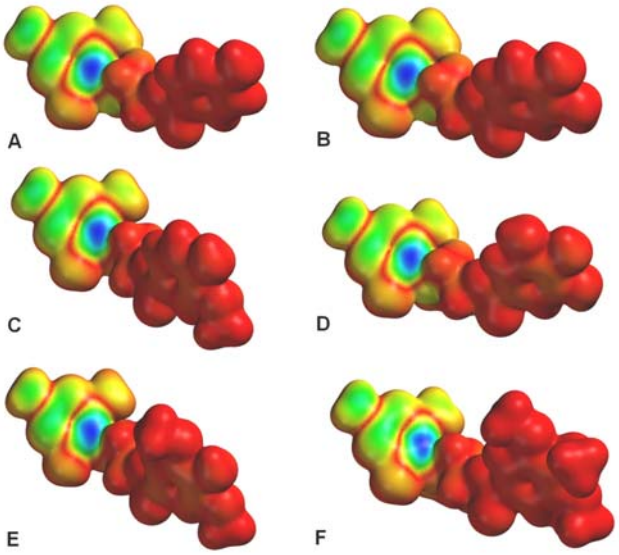

Figure 3. HOMO iso-density profiles of the hybrid compounds. Calculated at B3LYP/6-31G** basis-set levels.

4.3. Electronic property analysis

In order to better understand the molecular interactions and structural factors that may be involved in the activity of the designed hybrid compounds targeting both the enzymes, stereo-electronic properties such as molecular orbital energies (the highest occupied molecular orbital (HOMO) and lowest unoccupied molecular orbital (LUMO)), reactivity index or gap (difference between HOMO and LUMO energies) and molecular electrostatic potential (MEP) were calculated using the B3LYP/6-31g** density functional theory on the geometry optimized structures. Calculated absolute energies, reactivity indexes & electronic properties of the compounds are listed in Table 3. HOMO and LUMO orbital energies are related to ionization potential and electron affinity and their respective frontier orbitals are associated to the molecule's reactivity i.e., HOMO energy is susceptible to electrophilic attack (donate e^-) and LUMO energy susceptible to nucleophilic attack (accept e^-) (56). The reactivity index (band gap) of the compounds with small difference implies high reactivity and large difference implies low reactivity in reactions (57). The energy gap (HOMO – LUMO, in Table 3) of the proposed compounds was found to be within a smaller narrow range of -4.79 to -4.93, indicating that these energies permit electron transfer and exchange making the compounds very highly reactive and similar in nature.

Three dimensional HOMO and LUMO profiles over the Van der Waals surface and the molecular electrostatic potential mapped onto total electron density surface of all the hybrid compounds are shown in Figure 3-5. For the three dimensional HOMO orbitals (Figure 3) of all the compounds, the predominant HOMO (electron-rich) orbitals were consistently observed on the amino and hydroxyl substituted aromatic pyrimidine ring of the MANIC compound derivative, indicating strong electrophilic affinity and the most significant LUMO (electron-poor) orbitals (Figure 4) of all the compounds were consistently observed on the hydroxyl substituted aromatic ring of the phytochemicals (*p*HBA, PA, VA, GA, SA & EA), indicating the localization of strong electron acceptor elements and thereby susceptible to strong nucleophilic attack.

Additionally, the MEP is a useful descriptor for understanding electrophilic/nucleophilic sites as well as hydrogen bonding interactions. In general, the negative

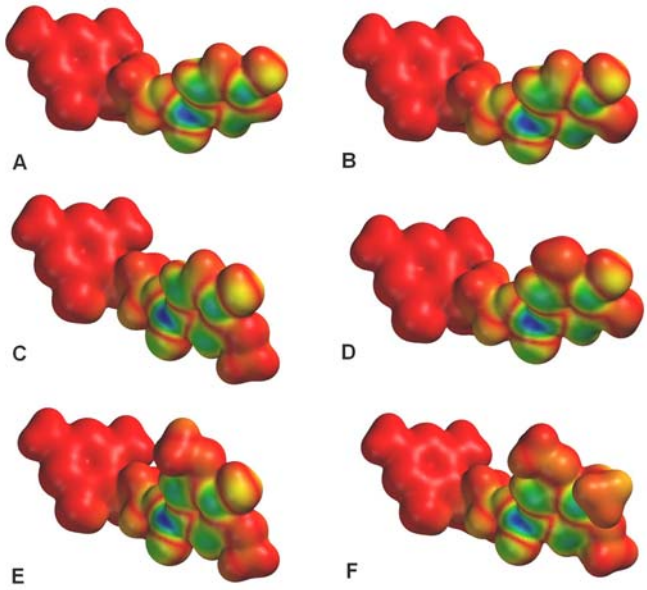

Figure 4. LUMO iso-density profiles of the hybrid compounds. Calculated at B3LYP/6-31G** basis-set levels.

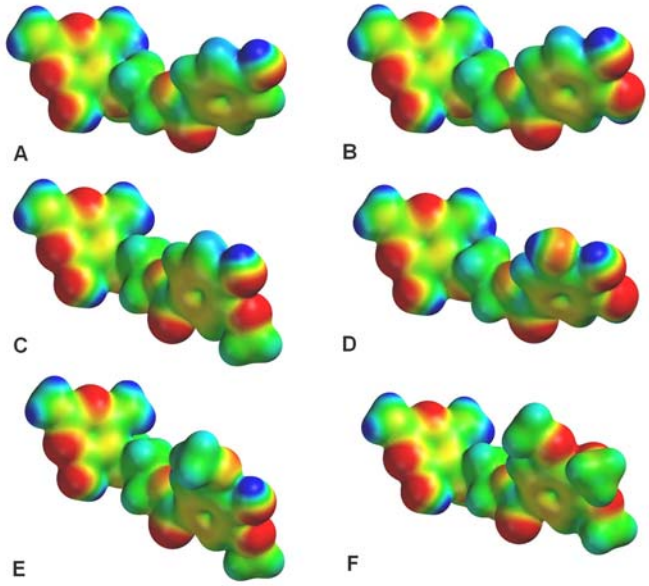

Figure 5. Molecular electrostatic potential (MEP) iso-density profiles of the hybrid compounds. Calculated at B3LYP/6-31G** basis-set levels.

potential sites (red color) of MEP represents regions of electrophilic reactivity and interaction through π-π bonding with the aromatic systems of interacting enzyme residues and positive potential sites (blue color) represents regions of nucleophilic reactivity (58). As expected, the predominant blue regions (positive potential sites) in the MEP profiles (Figure 5) of all the hybrid compounds are localized around the amino groups of the MANIC compound derivative indicating their hydrogen bond donor activity with the key active site residues in DHPS (Asn122, Asp192 and Asp103) and DHFR (Asp30, Ile8, Tyr110 and Ile104) enzymes. Also, the hydroxyl groups in the MANIC compound derivative and phytochemicals (*p*HBA, PA, VA, GA & SA) shows the presence of positive potential site (blue color) and negative potential site (red color), suggesting their role as both hydrogen bond donor and acceptor element that interacts with DHPS (Gly224 & Lys228) and DHFR (Asp30 & Arg55) active site residues. The predominant red regions (negative potential sites) in the MEP profiles (Figure 5) of all the compounds are localized around the methyl amino (nitrogen atom), oxygen and carbonyl oxygen atom in the carboxylic acid group and methoxy groups of the phytochemicals, participating in hydrogen bonding interaction with donor groups of key

active site residues in DHPS (Lys228, Arg262, Thr69 & Arg70) and DHFR (Arg55) enzymes. In addition, regions at the aromatic rings in all the compounds show red regions with decreasing intensity indicating weak positive electrostatic potential and thereby implying a hydrophobic nature of the aromatic rings. The above mentioned molecular orbitals and MEP profile features appear to be consistent with the key pharmacophoric features required for potent dual knockouts of both DHPS and DHFR enzymes.

4.4. Homology modeling and validation of the predicted structures

In order to study the binding modes of the designed hybrid compounds in *P. aeruginosa* DHPS and DHFR, we constructed the 3D structures of the two targets. The NCBI protein BLAST program was performed to search the homologous sequences of *P. aeruginosa* DHPS and DHFR with three dimensional structures deposited in the PDB. The BLASTp program resulted in sequence identity of 61% and 45% to *E. coli* DHPS (1AJ0) and DHFR (1RX3) and was chosen as suitable templates for comparative homology model building. The sequence alignment of the target and the template sequences obtained from CLUSTALW2 was used to build 3D models using, SWISS-MODEL (42) and MODELLER 9v7 (43) protein structure homology modeling tools. All the models obtained were subjected to WHATIF server to model missing side chains, to remove atomic clashes and to complete the protein structure (44). The RMSD of the generated homology models was calculated by structural superposition with their respective templates (1AJ0 and 1RX3) using SUPERPOSE (45) and the SWISS-MODEL constructed models resulted in lowest RMSD values, 0.18 Å (DHPS) and 0.39 Å (DHFR) respectively. RMSD values of ≤ 2 Å from the experimentally determined structures are considered as "highly accurate" models, while models with Cα RMSD above this threshold and ≤ 4 Å were termed "reliable" models and such models are not fit for drug design and binding affinity analysis (59). Thus, low RMSD values obtained shows the selected homology models are acceptable and similar to their respective templates.

The quality of the obtained *P. aeruginosa* DHPS and DHFR homology models were evaluated based on stereo-chemical analysis using PROCHECK (60), absolute measures on the geometry and energy profiles independently using QMEAN (61) and ANOLEA (62) available in the SWISS-MODEL Workspace (42) along with Verify3D (47) and PROSA (46). The Ramachandran plot produced from PROCHECK analysis showed 89% (DHPS) and 86.5% (DHFR) amino acid residues within the most favored regions, 11% (DHPS) and 13.5% (DHFR) within additionally allowed regions indicating that the models have good overall stereo-chemical quality (Figure 11(a,b)). The QMEAN analysis used for the estimation of the global quality of the entire models as well as for the local per-residue analysis of different regions within the models resulted in the QMEAN6 global score values 0.833 (DHPS) and 0.752 (DHFR) which are well with the quality range (0 - 1) with higher values for better models (61). In addition to this, QMEAN Z-scores estimated represents a measure of the absolute quality of the models by providing an estimate to scores obtained for high-resolution reference structures solved experimentally by X-ray crystallography, models with low quality are expected to have strong negative Z-scores and "Good structures" have (mean Z-scores = - 0.65) (63). The observed Z-score values for the predicted models were 0.69 (DHPS) and -0.077 (DHFR), suggesting these models are of comparable quality to high-resolution experimental structures. The energy profiles of the models were estimated using both ANOLEA and PROSA analysis showed regions with predominant low energy (negative values). The PROSA tool is widely used to check 3D models of protein structures for potential errors by calculating z-score and a plot of its residue energies, z-score value is displayed in a plot that contains the *z*-scores of all experimentally determined protein chains in current PDB and models with z-scores outside the range characteristic for native proteins indicate erroneous structures, while the energy plot shows the local model quality by plotting residue energies as a function of amino acid sequence position in which positive values correspond to problematic or erroneous parts of a model (46). The calculated z-scores -7.93 (DHPS) and -5.19 (DHFR) of the modeled structures are within the range of scores typically found for native proteins of similar size and the energy plot showed all the residues in DHPS have negative energies while in DHFR majority of the residues showed negative energy and very few residues displayed positive energy values (Figure 11(c,d)). Finally, Verify3D was used to test the accuracy of a 3D model by comparing the model to its own amino-acid sequence using a 3D profile (47). The average 3D-1D profile scores for the model (DHPS, 0.76) and that of its template were very close (1AJ0, 0.82) similarly, (DHFR, 0.69) and its template (1RX3, 0.71). Hence, the validation based on the geometry, energy profiles and overall stereo-chemical quality suggests that the homology models obtained are of high quality and appropriate for further protein-ligand interaction studies.

4.5. Molecular docking

In order to gain insights into the binding modes of the designed hybrid compounds in both DHPS and DHFR enzymes, molecular docking studies were carried out using the Molegro virtual docker program (48). The docking results of all the proposed compounds along with DHPPP (DHPS substrate)/methotrexate (DHFR inhibitor) in *P. aeruginosa* DHPS & DHFR are ranked based on their binding affinity scores (Table 4 & 5).

4.5.1. Docking of DHPPP and proposed compounds at the pterin binding site of DHPS

The modeled *P. aeruginosa* DHPS is folded into an eight stranded α/β TIM barrel structure i.e., eight α-helices stacked around the outside of an inner cylinder of parallel β-strands in which the pterin pyrophosphate (DHPPP) binding site is in the deep cleft located towards the C-terminal end of the β-strands, similar to the crystal structure of *E. coli* DHPS (64). The dihydropterin group in DHPPP is stabilized in the narrow pocket by hydrogen bond interactions with Asn122, Asp192, Asp103 and Lys228 and non-polar interactions with Val124, Met146, Phe195, Phe197, Gly224, Lys228 and Arg262 (Figure 6a).

Table 4. Docking results of DHPPP and designed hybrid compounds (ranked on the basis of binding affinity scores) at the pterin binding pocket of *P. aeruginosa* DHPS.

Compounds	Scoring function		E_{Inter}[3]	E_{Intra}[4]	Hbond[5]	LE1[6]	LE3[7]	Binding affinity (kJ/mol)	Residues involved in Hydrogen bonding
	MolDock[1]	Rerank[2]							
HD_EA	-130.71	-72.01	-153.86	23.15	-21.25	-4.67	-2.57	-41.3	Asp 192, Asn122, Asp103, Arg262, Gly224, Lys228, Thr69, Arg70
HD_SA	-125.86	-70.35	-147.26	21.39	-20.79	-4.66	-2.61	-36.76	Asp 192, Asn122, Asp103, Arg262, Gly224, Lys228, Thr69, Arg70
HD_VA	-117.96	-60.27	-138.01	20.04	-21.18	-4.72	-2.41	-34.64	Asp 192, Asn122, Asp103, Arg262, Gly224, Lys228, Thr69, Arg70
HD_*p*HBA	-107.34	-47.59	-125.94	18.6	-20.52	-4.67	-2.07	-32.01	Asp 192, Asn122, Asp103, Arg262, Gly224, Lys228, Thr69, Arg70
HD_PA	-109.99	-44.49	-130.69	20.69	-20.47	-4.58	-1.85	-29.85	Asp 192, Asn122, Asp103, Arg262, Gly224, Lys228, Thr69, Arg70
HD_GA	-112.28	-58.33	-134.26	21.98	-20.47	-4.49	-2.33	-27.73	Asp 192, Asn122, Asp103, Arg262, Gly224, Lys228, Thr69, Arg70
DHPPP	-116.91	-96.71	-123.89	6.982	-29.33	-5.31	-4.39	-33.33	Asp 192, Asn122, Asp103, Lys228, Arg262, Thr69, Arg70, Asn29, His264

[1]MolDock: docking score function by MolDock, [2]Rerank: reranking score function, [3]E_{Inter}: ligand – protein (DHPS) interaction energy, [4]E_{Intra}: internal energy of the ligand, [5]HBond: hydrogen bonding energy, [6]LE1: Ligand efficiency 1 - MolDock score divided by Heavy atoms count, [7]LE3: Ligand efficiency 3 – Rerank score divided by Heavy atoms count, DHPPP (dihydropterin pyrophosphate) – DHPS substrate.

Table 5. Docking results of methotrexate and designed hybrid compounds (ranked on the basis of binding affinity scores) at the folate binding site in *P. aeruginosa* DHFR.

Compounds	Scoring function		E_{Inter}[3]	E_{Intra}[4]	Hbond[5]	LE1[6]	LE3[7]	Binding affinity (kJ/mol)	Residues involved in Hydrogen bonding
	MolDock[1]	Rerank[2]							
HD_EA	-103.54	-85.61	-123.33	19.78	-14.83	-3.69	-3.08	-37.56	Asp30, Ala10, Ile8, Tyr110, Ile104, Arg55
HD_SA	-104.16	-84.21	-119.21	15.05	-15.28	-3.86	-3.12	-33.16	Asp30, Ala10, Ile8, Tyr110, Ile104, Arg55
HD_VA	-96.96	-79.34	-111.95	14.99	-12.35	-3.88	-3.17	-29.59	Asp30, Ala10, Ile8, Tyr110, Ile104, Arg55
HD_*p*HBA	-87.69	-70.28	-103.38	15.69	-12.06	-3.81	-3.06	-27.28	Asp30, Ala10, Ile8, Tyr110, Ile104, Arg55
HD_PA	-94.39	-80.44	-109.33	14.94	-13.77	-3.93	-3.35	-25.89	Asp30, Ala10, Ile8, Tyr110, Ile104, Arg55
HD_GA	-92.78	-76.62	-112.44	19.66	-15.48	-3.71	-3.06	-24.53	Asp30, Ala10, Ile8, Tyr110, Ile104, Arg55
MTX	-151.34	-119.61	-174.19	22.85	-18.08	-4.48	-3.54	-33.05	Asp30, Ile8, Ile104, Tyr110, Arg55, Arg60

[1]MolDock: docking score function by MolDock, [2]Rerank: reranking score function, [3]E_{Inter}: ligand – protein (DHPS) interaction energy, [4]E_{Intra}: internal energy of the ligand, [5]HBond: hydrogen bonding energy, [6]LE1: Ligand efficiency 1 - MolDock score divided by Heavy atoms count, [7]LE3: Ligand efficiency 3 – Rerank score divided by Heavy atoms count, MTX (methotrexate) – DHFR inhibitor.

The α-phosphate group makes hydrogen bond interactions with Thr69 while the β-phosphate group involves in hydrogen bond interactions with Asn29, Arg70, Arg262 and His264 (Figure 6a).

Since, the active site residues of the DHPPP substrate binding pocket are highly conserved in both prokaryotic and lower eukaryotic DHPS enzymes, inhibitors designed to bind to this site are predicted to have a broad spectrum of activity and also less likely to develop drug resistance mutations (64). The docking results show that the proposed hybrid compounds have similar binding conformations and good binding affinities at the pterin binding pocket of DHPS maintaining contacts with all the key conserved residues required for inhibition. The major residues participating in hydrogen bond interactions with the designed inhibitors in the DHPS active site are tabulated in Table 4 based on their respective binding affinity scores.

Considering the top ranked compound HD_EA, the pyrimidine ring engages the pterin binding pocket and the hydroxyl moiety forms hydrogen bonds with Gly224 and Lys228, the unsubstituted amine at the 2-position forms hydrogen bond interactions with Asp192 and Asn122 while the nitrogen at the 3-position also contacts the Asn122 residue, the unsubstituted amine at the 6-position interacts with Asp103, the nitrogen atom at the 5-position engages in hydrogen bond interaction with Lys228 and Arg262 at the base of the pocket (Figure 7a). In addition, the N-methyl group with Arg262 and the linker group with Phe197 residue make Van der Waals interactions. The linker group attached to the phytochemical extends the ring adopting the conformation similar to the *p*ABA moiety which brings it closer to interact with Thr69 and Arg70 by hydrogen bonding (Figure 7a). The docking calculations also demonstrated that the pyrimidine ring and phytochemical moiety in all the designed hybrid compounds engage in similar interactions at the pterin binding pocket of DHPS (Figure 7b).

4.5.2. Docking of methotrexate and proposed compounds at the folate binding site of DHFR

The fold of the modeled *P. aeruginosa* DHFR contains a mixed seven parallel stranded β-sheet and one C-terminal antiparallel strand with four flanking α-helices, similar to the crystal structure of *E. coli* DHPS (65). Despite the low sequence identity of only 30% between different species of DHFRs, the active site characteristics of all the structures is highly conserved and similar (66). The 2,4-diaminopteridine ring of methotrexate is situated into a deep hydrophobic pocket of the active site cavity

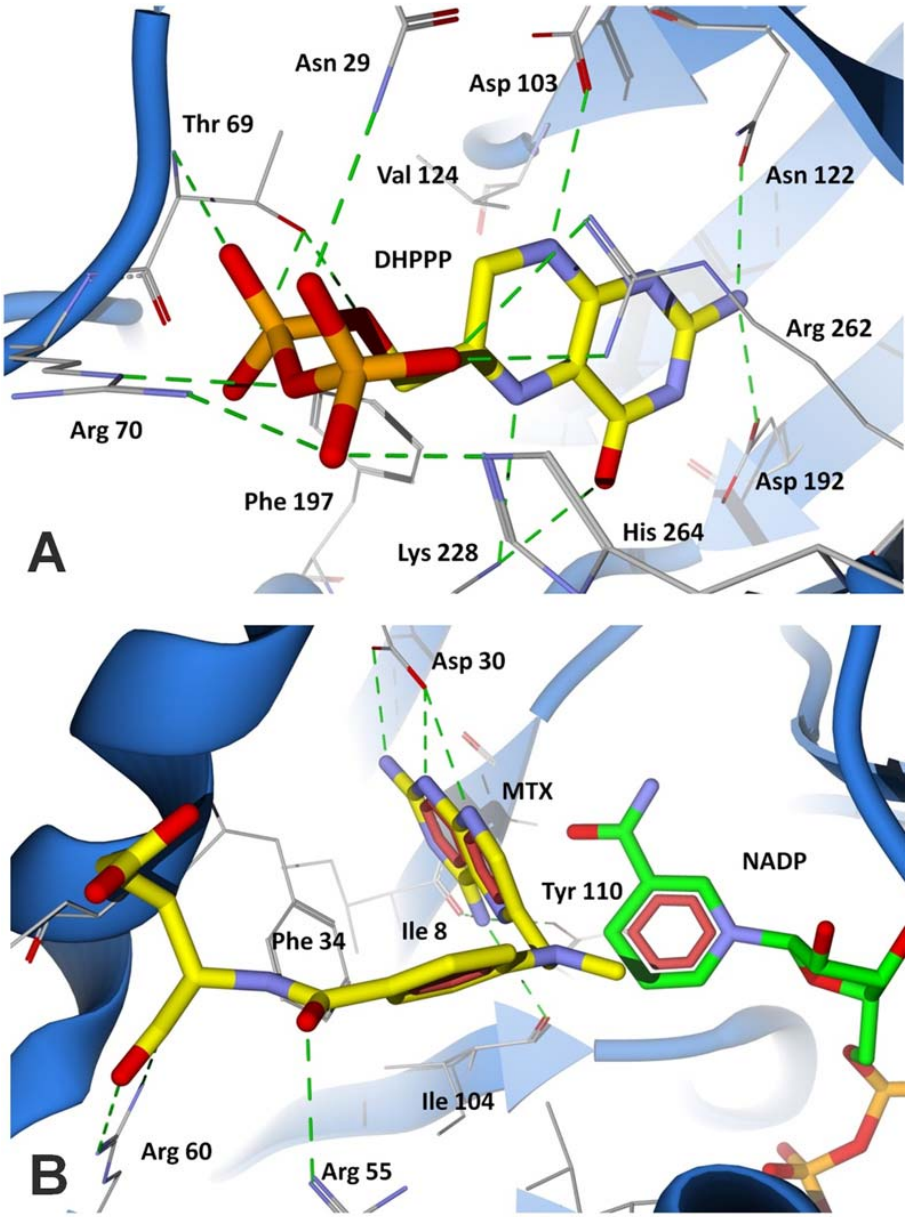

Figure 6. Binding modes of DHPPP and methotrexate in *P. aeruginosa* DHPS and DHFR active site cavities, obtained from docking studies. (A) The substrate of DHPS (DHPPP) (yellow stick model) docked at pterin binding site of DHPS; (B) DHFR inhibitor methotrexate (yellow stick model) docked at folate binding site of DHFR and the cofactor NADP is shown as green stick model. The residues are shown as wireframe colored by their element and the hydrogen bonds are illustrated as dotted green lines.

with 2-amino group and N1 forming hydrogen bonds with Asp30 while 4-amino group engages in strong hydrogen bond interactions with the main chain carbonyl oxygen atom of Ile8, Ile104 and the hydroxyl group of Tyr110 (Figure 6b).

The phenyl group in the *p*ABA ring of methotrexate forms Van der Waals contacts with Phe34, Leu53 and Leu57 residues. The carbonyl group in the *p*ABA moiety forms hydrogen bonding with Arg55 residue and the glutamate tail forms salt bridge interactions with Arg60 at the end of the pocket (Figure 6b). The docking results show that all the proposed hybrid compounds have a good fit into the folate binding site of DHFR and are positioned in a way similar to the inhibitor (methotrexate) (Figure 8b). The major residues participating in hydrogen bond interactions with the designed inhibitors in the DHFR active site are tabulated in Table 5. The pyrimidine ring of the hybrid compound HD_EA engage the folate binding site and interacts through six major hydrogen bonds (Figure 8a). The 2-amino and 4-hydroxyl group engages with Asp30 while the Ala 10 residue interacts via the nitrogen

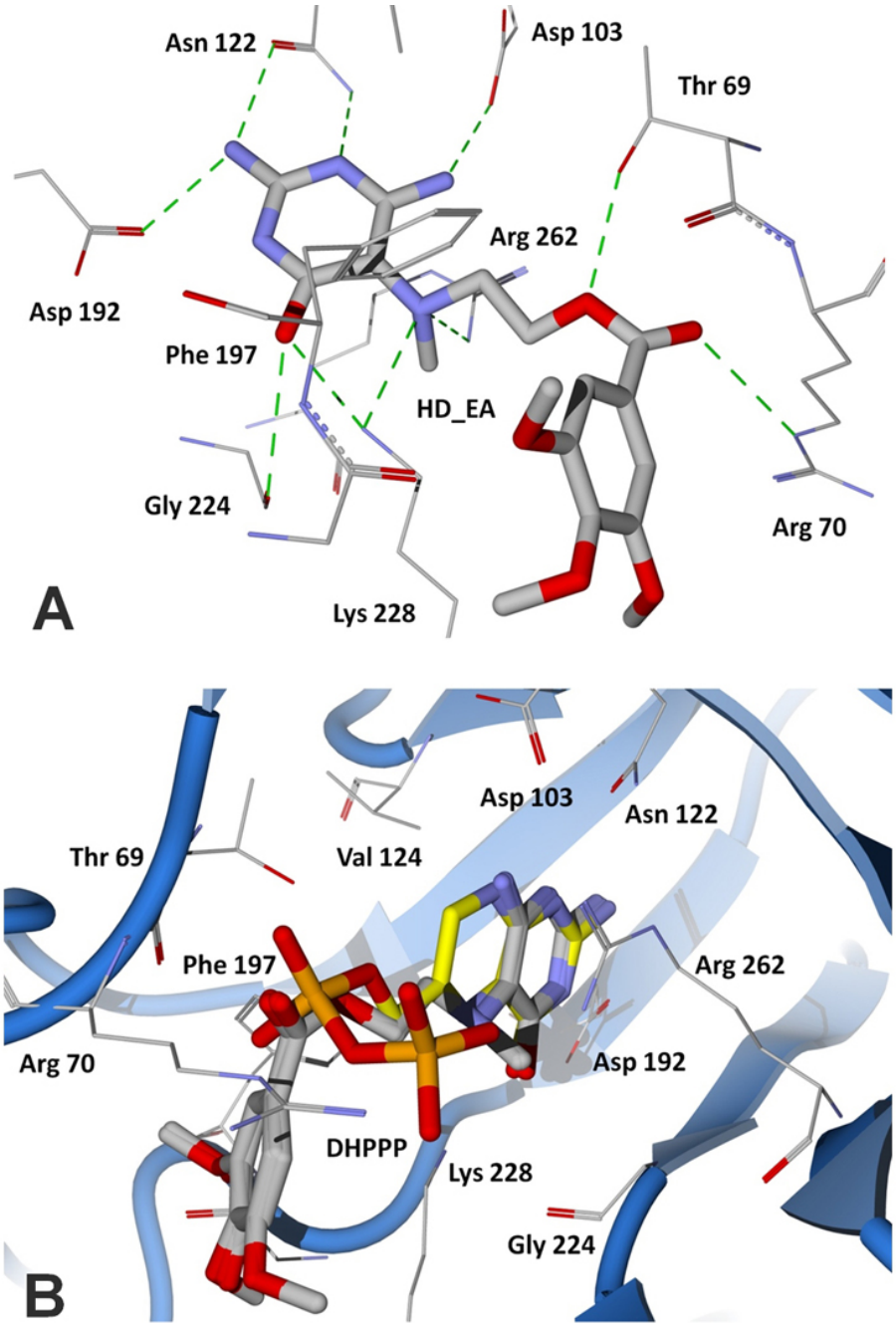

Figure 7. Docking of designed hybrid compounds at pterin binding site of *P. aeruginosa* DHPS. (A) Binding pose of the top-scored compound HD_EA (grey stick model); (B) Binding poses of all the designed hybrid compounds (grey stick models) superimposed with DHPPP (yellow stick model). The residues are shown as wireframe colored by their element and the hydrogen bonds are illustrated as dotted green lines.

atom at the 1-position of the pyrimidine ring and the 6-amino group interacts with Ile8, Tyr110 and Ile104 residues. The pyrimidine ring also makes Van der Waals interactions with Phe34, Ile8, Ala9 and Ala10. The trimethoxybenzyl group of the phytochemical interacts via Van der Waals contacts with Phe34, Leu53 and Leu57 (Figure 8a). In addition, the methoxy groups in the phytochemical ring of HD_EA forms hydrogen bond interactions with the conserved Arg55 residue.

4.6. Molecular dynamics simulations

To further rationalize the stability of the unbound enzyme complexes (I – DHPS and IV - DHFR), ligand-bound enzyme complexes (II - DHPPP-DHPS and V -

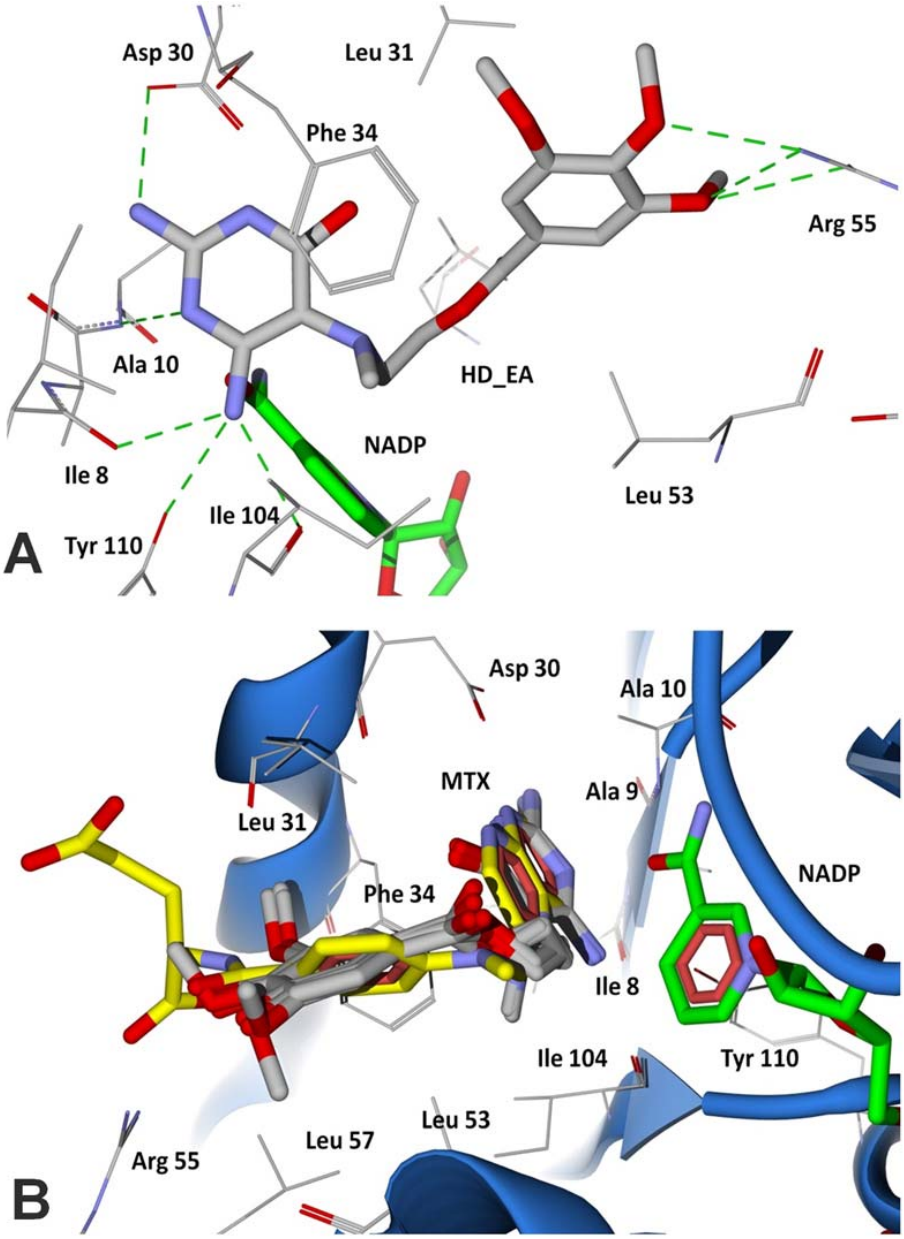

Figure 8. Docking of designed hybrid compounds at folate binding site of *P. aeruginosa* DHFR. (A) Binding pose of the top-scored compound HD_EA (grey stick model); (B) Binding poses of all the designed hybrid compounds (grey stick models) superimposed with methotrexate (yellow stick model) and cofactor NADP represented as green stick model. The residues are shown as wireframe colored by their element and the hydrogen bonds are illustrated as dotted green lines.

MTX-NADP-DHFR) and top ranked hybrid compound-bound enzyme complexes (III - HD_EA-DHPS and VI - HD_EA-NADP-DHFR) the conformational changes with respect to the initial structure were analyzed by RMSD during 3000 ps simulation time (Figure 9a & 9b). The main chain average RMSD values obtained for the trajectories of the enzyme complexes I & IV were about 1.44 Å and 1.972 Å, for complexes II & V were 1.488 Å and 2.095 Å and complexes III & VI were 1.661 Å and 1.854 Å, respectively. As can be seen in the plots that after 500 ps, all the complexes tends to converge with low values of deviation of the molecules with respect to the original atomic positions, indicating the systems are stable and equilibrated.

Furthermore, analyses of the root mean square fluctuation of key active site residues versus the residue number for all the complexes are shown in Figure 10 (a-d). The RMSF value illustrates the average displacement of each residue in relation to their average backbone structure over the whole simulation and indicates the relative flexibility that describes each of these residue elements. As

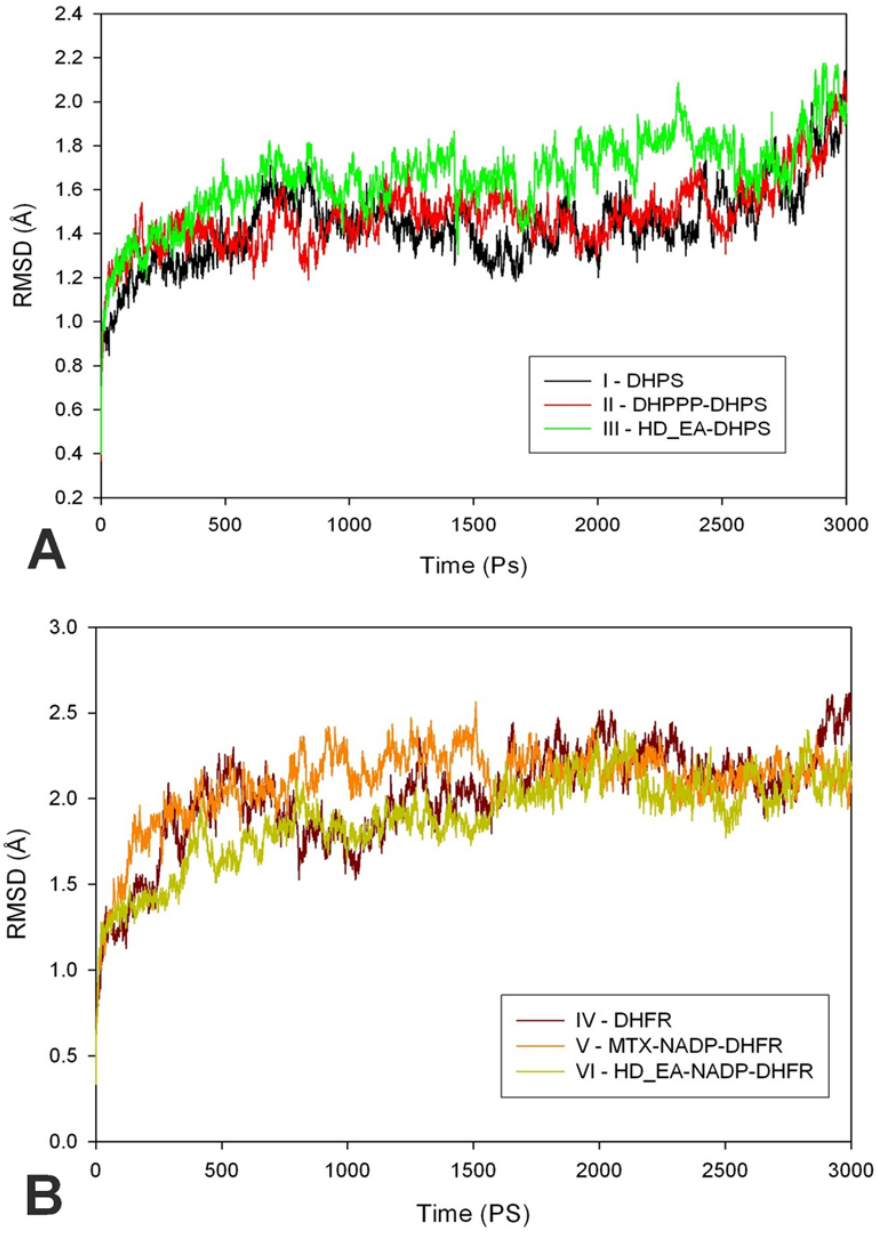

Figure 9. Root mean square deviation (RMSD) of backbone C^{α} atoms of the complexes versus time in picoseconds. (A) Unbound DHPS complex - I, DHPPP bound DHPS complex - II and top-scored hybrid compound HD_EA bound DHPS complex - III; (B) Unbound DHFR complex – IV, methotrexate and cofactor NADP bound DHFR complex – V and top-scored hybrid compound HD_EA and cofactor NADP bound DHFR complex – VI.

expected, the RMSF plots of all the complexes indicate that the main backbone residues with high fluctuations are those in the flexible loops. The residue positions between 34 and 41 and the turn which includes residues in positions between 237 and 241 of complexes I – DHPS, II – DHPPP-DHPS and III – HD_EA-DHPS shows high fluctuations (Figure 10a). Similarly, the complexes IV – DHFR, V – MTX-NADP-DHFR and VI – HD_EA-NADP-DHFR shows loops that includes residues between 67 and 78 and the α-helix structure which includes residues in positions between 90 and 96 which is located away from the binding site cavity, show high fluctuations (Figure 10b). The mobile flexibilities (RMSF) values of key active site residues in each complex fluctuates widely from 0.5 Å to 2.4 Å, indicating that the active site residue elements maintain their positions in relation to their corresponding enzyme complexes (Figure 10c & 10d). In comparison to the unbound complexes (I – DHPS and IV - DHFR), both ligand bound complexes (II – DHPPP-DHPS and V – MTX-NADP) and inhibitor bound complex (III – HD_EA-DHPS and VI – HD_EA-DHFR) showed smaller RMSF values indicating tight interaction between active site

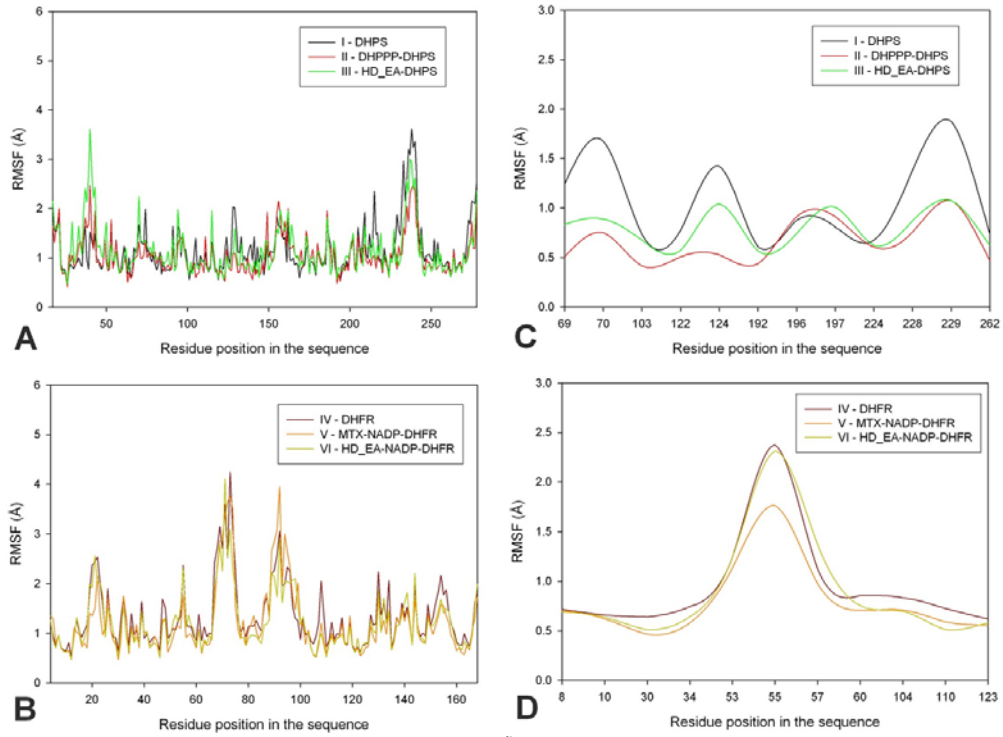

Figure 10. Root mean square fluctuation (RMSF) of backbone C^{α} atoms of the complexes versus residue number in the sequence. (A) Unbound DHPS complex - I, DHPPP bound DHPS complex - II and top-scored hybrid compound HD_EA bound DHPS complex - III; (B) Unbound DHFR complex – IV, methotrexate and cofactor NADP bound DHFR complex – V and top-scored hybrid compound HD_EA and cofactor NADP bound DHFR complex – VI; (C) Closer look of DHPS active site residues RMSF during the simulation of three complexes; (D) Closer look of DHFR active site residues RMSF during the simulation of three complexes.

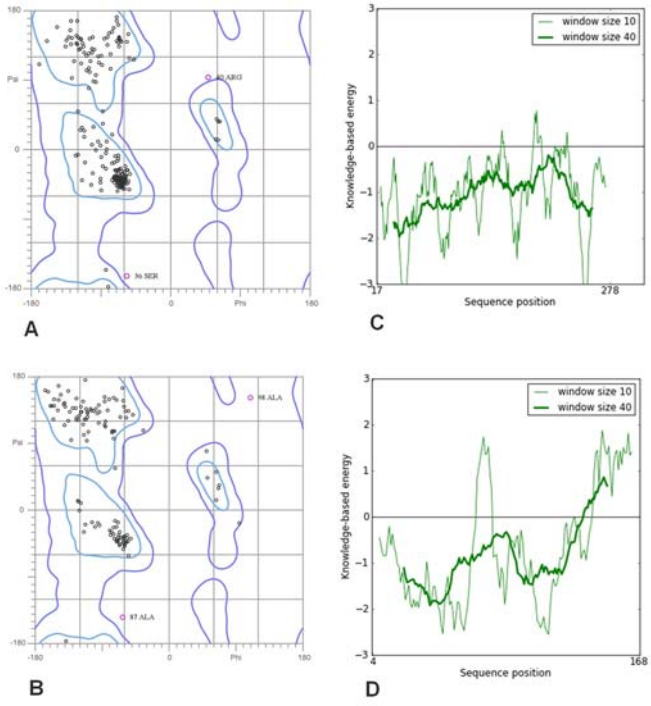

Figure 11. Validation of *P. aeruginosa* DHPS/DHFR homology models (A) DHPS & (B) DHFR Ramachandran plots; (C) DHPS & (D) DHFR PROSA energy plots.

residues. Thus, the low RMSD and RMSF deviations indicate that the inhibitor bound dual enzyme complexes are stable and preserve the inhibitor interactions shown in the molecular docking experiments.

5. CONCLUSION

In summary, the present work describes the design hypothesis of novel dual action hybrid compounds for synergistic blockage of two different enzymes DHPS and DHFR in the folate biosynthesis pathway using various integrated *in silico* based methods. This viable hybrid design framework is particularly important as it combines molecular tinkering of natural product by optimization through structural modifications thereby restricting unwanted off-target effects with the approach to overcome the existing resistance mechanisms and delay the resistance development of multi-drug resistant pathogens due to subsequent addressing of two different targets. These compounds are potential drug candidates and further studies are necessary to support the theoretical analysis, so experimental evaluations are underway in our laboratories. Thus, identification and modification of most biologically active promiscuous plant-derived natural products with the view to improve and balance their drug-like properties will offer novel agents with superior therapeutic properties against infectious diseases.

6. ACKNOWLEDGEMENTS

PJ, MKS and SKD conceived the study, designed the methods, carried out the data analysis and drafted the manuscript. MKS supervised the research and contributed to drafting the manuscript, LCD, KRS, SKD and MIS gave useful suggestions and improved on it. All authors have read and approved the final manuscript.

7. REFERENCES

1. E. B. M. Breidenstein, C. de la Fuente-Núñez and R. E. W. Hancock: Pseudomonas aeruginosa: All roads lead to resistance. *Trends in Microbiology*, 19(8), 419-426 (2011)

2. P. A. Lambert: Mechanisms of antibiotic resistance in Pseudomonas aeruginosa. *Journal of the Royal Society of Medicine, Supplement*, 95(41), 22-26 (2002)

3. H. W. Boucher, G. H. Talbot, J. S. Bradley, J. E. Edwards, D. Gilbert, L. B. Rice, M. Scheld, B. Spellberg and J. Bartlett: Bad Bugs, No Drugs: No ESKAPE! An Update from the Infectious Diseases Society of America. *Clinical Infectious Diseases*, 48(1), 1-12 (2009) doi:10.1086/595011

4. M. G. Page and J. Heim: Prospects for the next anti-Pseudomonas drug. *Current Opinion in Pharmacology*, 9(5), 558-565 (2009)

5. H. Brötz-Oesterhelt and N. A. Brunner: How many modes of action should an antibiotic have? *Current Opinion in Pharmacology*, 8(5), 564-573 (2008)

6. A. L. Hopkins: Network pharmacology: The next paradigm in drug discovery. *Nature Chemical Biology*, 4(11), 682-690 (2008)

7. V. Pokrovskaya and T. Baasov: Dual-acting hybrid antibiotics: A promising strategy to combat bacterial resistance. *Expert Opinion on Drug Discovery*, 5(9), 883-902 (2010)

8. R. Morphy and Z. Rankovic: Designing multiple ligands - Medicinal chemistry strategies and challenges. *Current Pharmaceutical Design*, 15(6), 587-600 (2009)

9. R. Morphy and Z. Rankovic: Fragments, network biology and designing multiple ligands. *Drug Discovery Today*, 12(3-4), 156-160 (2007)

10. E. Chamot, E. B. El Amari, P. Rohner and C. Van Delden: Effectiveness of combination antimicrobial therapy for Pseudomonas aeruginosa bacteremia. *Antimicrobial Agents and Chemotherapy*, 47(9), 2756-2764 (2003)

11. M. Bassetti, E. Righi and C. Viscoli: Pseudomonas aeruginosa serious infections: Mono or combination antimicrobial therapy? *Current Medicinal Chemistry*, 15(5), 517-522 (2008)

12. S. J. Johnson, E. J. Ernst and K. G. Moores: Is double coverage of gram-negative organisms necessary? *American Journal of Health-System Pharmacy*, 68(2), 119-124 (2011)

13. K. A. Traugott, K. Echevarria, P. Maxwell, K. Green and J. S. Lewis Ii: Monotherapy or combination therapy? The Pseudomonas aeruginosa conundrum. *Pharmacotherapy*, 31(6), 598-608 (2011)

14. H. Labischinski, J. Cherian, C. Calanasan and R. S. Boyce: Hybrid Antimicrobial Compounds and Their Use. In, (2010)

15. V. Pokrovskaya, V. Belakhov, M. Hainrichson, S. Yaron and T. Baasov: Design, synthesis, and evaluation of novel fluoroquinolone - Aminoglycoside hybrid antibiotics. *Journal of Medicinal Chemistry*, 52(8), 2243-2254 (2009)

16. S. Bera, G. G. Zhanel and F. Schweizer: Evaluation of amphiphilic aminoglycoside-peptide triazole conjugates as antibacterial agents. *Bioorganic and Medicinal Chemistry Letters*, 20(10), 3031-3035 (2010)

17. G. R. Zimmermann, J. Lehár and C. T. Keith: Multi-target therapeutics: when the whole is greater than the sum of the parts. *Drug Discovery Today*, 12(1-2), 34-42 (2007)

18. S. Hawser, S. Lociuro and K. Islam: Dihydrofolate reductase inhibitors as antibacterial agents. *Biochemical Pharmacology*, 71(7), 941-948 (2006)

19. P. Huovinen: Resistance to trimethoprim-sulfamethoxazole. *Clinical Infectious Diseases*, 32(11), 1608-1614 (2001)

20. T. Köhler, M. Kok, M. Michea-Hamzehpour, P. Plesiat, N. Gotoh, T. Nishino, L. K. Curty and J. C. Pechere: Multidrug efflux in intrinsic resistance to trimethoprim and sulfamethoxazole in Pseudomonas aeruginosa. *Antimicrobial Agents and Chemotherapy*, 40(10), 2288-2290 (1996)

21. S. P. James, I. Jamie, S. S. Ian, M.: Folate Biosynthesis - Reappraisal of Old and Novel Targets in the Search for New Antimicrobials. *The Open Enzyme Inhibition Journal*, 1, 12-33 (2008)

22. K. E. Hevener, M. K. Yun, J. Qi, I. D. Kerr, K. Babaoglu, J. G. Hurdle, K. Balakrishna, S. W. White and R. E. Lee: Structural studies of pterin-based inhibitors of dihydropteroate synthase. *Journal of Medicinal Chemistry*, 53(1), 166-177 (2010)

23. B. C. Bennett, H. Xu, R. F. Simmerman, R. E. Lee and C. G. Dealwis: Crystal structure of the anthrax drug target, Bacillus anthracis dihydrofolate reductase. *Journal of Medicinal Chemistry*, 50(18), 4374-4381 (2007)

24. M. D. Navarro-Martínez, E. Navarro-Perán, J. Cabezas-Herrera, J. Ruiz-Gómez, F. García-Cánovas and J. N. Rodríguez-López: Antifolate activity of epigallocatechin gallate against Stenotrophomonas maltophilia. *Antimicrobial Agents and Chemotherapy*, 49(7), 2914-2920 (2005)

25. P. Jayaraman, K. R. Sakharkar, L. C. Sing, V. T. K. Chow and M. K. Sakharkar: Insights into antifolate activity of phytochemicals against Pseudomonas aeruginosa. *Journal of Drug Targeting*, 19(3), 179-188 (2011)

26. P. Jayaraman, M. K. Sakharkar, C. S. Lim, T. H. Tang and K. R. Sakharkar: Activity and interactions of antibiotic and phytochemical combinations against pseudomonas aeruginosa *in vitro*. *International Journal of Biological Sciences*, 6(6), 556-568 (2010)

27. M. K. Sakharkar, P. Jayaraman, W. M. Soe, V. T. K. Chow, L. C. Sing and K. R. Sakharkar: *In vitro* combinations of antibiotics and phytochemicals against Pseudomonas aeruginosa. *Journal of Microbiology, Immunology and Infection*, 42(5), 364-370 (2009)

28. S. Gibbons, E. Moser and G. W. Kaatz: Catechin gallates inhibit multidrug resistance (MDR) in Staphylococcus aureus. *Planta Medica*, 70(12), 1240-1242 (2004)

29. S. Hemaiswarya, A. K. Kruthiventi and M. Doble: Synergism between natural products and antibiotics against infectious diseases. *Phytomedicine*, 15(8), 639-652 (2008)

30. J. M. Rollinger: Accessing target information by virtual parallel screening-The impact on natural product research. *Phytochemistry Letters*, 2(2), 53-58 (2009)

31. M. Saleem, M. Nazir, M. S. Ali, H. Hussain, Y. S. Lee, N. Riaz and A. Jabbar: Antimicrobial natural products: An update on future antibiotic drug candidates. *Natural Product Reports*, 27(2), 238-254 (2010)

32. F. E. Koehn and G. T. Carter: The evolving role of natural products in drug discovery. *Nature Reviews Drug Discovery*, 4(3), 206-220 (2005)

33. D. J. Newman and G. M. Cragg: Natural Products As Sources of New Drugs over the 30 Years from 1981 to 2010. *Journal of Natural Products* (2012) doi:10.1021/np200906s

34. A. Ganesan: The impact of natural products upon modern drug discovery. *Current Opinion in Chemical Biology*, 12(3), 306-317 (2008)

35. T. P. T. Cushnie and A. J. Lamb: Antimicrobial activity of flavonoids. *International Journal of Antimicrobial Agents*, 26(5), 343-356 (2005)

36. X. H. Ma, Z. Shi, C. Tan, Y. Jiang, M. L. Go, B. C. Low and Y. Z. Chen: In-silico approaches to multi-target drug discovery : computer aided multi-target drug design, multi-target virtual screening. *Pharm Res*, 27(5), 739-49 (2010) doi:10.1007/s11095-010-0065-2 [doi]

37. P. Agarwal and D. B. Searls: Literature mining in support of drug discovery. *Briefings in Bioinformatics*, 9(6), 479-492 (2008)

38. R. Guha, M. T. Howard, G. R. Hutchison, P. Murray-Rust, H. Rzepa, C. Steinbeck, J. Wegner and E. L. Willighagen: The Blue ObeliskInteroperability in Chemical Informatics. *Journal of Chemical Information and Modeling*, 46(3), 991-998 (2006) doi:10.1021/ci050400b

39. I. Wavefunction: SPARTAN. In, 18401 Von Karman Avenue, Suite 370 Irvine, CA 92612 USA (2010)

40. W. Koch and M. C. Holthausen. *A Chemist's Guide to Density Functional Theory* (2000)

41. Y. H. Zhao, M. H. Abraham, J. Le, A. Hersey, C. N. Luscombe, G. Beck, B. Sherborne and I. Cooper: Rate-limited steps of human oral absorption and QSAR studies. *Pharmaceutical Research*, 19(10), 1446-1457 (2002)

42. K. Arnold, L. Bordoli, J. Kopp and T. Schwede: The SWISS-MODEL workspace: A web-based environment for protein structure homology modelling. *Bioinformatics*, 22(2), 195-201 (2006)

43. A. Sali and T. L. Blundell: Comparative protein modelling by satisfaction of spatial restraints. *Journal of Molecular Biology*, 234(3), 779-815 (1993)

44. R. Rodriguez, G. Chinea, N. Lopez, T. Pons and G. Vriend: Homology modeling, model and software evaluation: Three related resources. *Bioinformatics*, 14(6), 523-528 (1998)

45. R. Maiti, G. H. Van Domselaar, H. Zhang and D. S. Wishart: SuperPose: A simple server for sophisticated

structural superposition. *Nucleic Acids Research*, 32(WEB SERVER ISS.), W590-W594 (2004)

46. M. Wiederstein and M. J. Sippl: ProSA-web: interactive web service for the recognition of errors in three-dimensional structures of proteins. *Nucleic Acids Research*, 35(Web Server issue), W407-410 (2007)

47. D. Eisenberg, R. Lüthy and J. U. Bowie: VERIFY3D: Assessment of protein models with three-dimensional profiles. In, (1997)

48. R. Thomsen and M. H. Christensen: MolDock: A new technique for high-accuracy molecular docking. *Journal of Medicinal Chemistry*, 49(11), 3315-3321 (2006)

49. R. Wang, X. Fang, Y. Lu and S. Wang: The PDBbind database: Collection of binding affinities for protein-ligand complexes with known three-dimensional structures. *Journal of Medicinal Chemistry*, 47(12), 2977-2980 (2004)

50. E. Krieger, T. Darden, S. B. Nabuurs, A. Finkelstein and G. Vriend: Making optimal use of empirical energy functions: Force-field parameterization in crystal space. *Proteins: Structure, Function and Genetics*, 57(4), 678-683 (2004)

51. U. Essmann, L. Perera, M. L. Berkowitz, T. Darden, H. Lee and L. G. Pedersen: A smooth particle mesh Ewald method. *The Journal of Chemical Physics*, 103(19), 8577-8593 (1995)

52. E. Krieger, J. E. Nielsen, C. A. E. M. Spronk and G. Vriend: Fast empirical pKa prediction by Ewald summation. *Journal of Molecular Graphics and Modelling*, 25(4), 481-486 (2006)

53. M. G. Lerner, A. L. Bowman and H. A. Carlson: Incorporating dynamics in E. coli dihydrofolate reductase enhances structure-based drug discovery. *Journal of Chemical Information and Modeling*, 47(6), 2358-2365 (2007)

54. C. A. Lipinski: Lead- and drug-like compounds: The rule-of-five revolution. *Drug Discovery Today: Technologies*, 1(4), 337-341 (2004)

55. D. F. Veber, S. R. Johnson, H. Y. Cheng, B. R. Smith, K. W. Ward and K. D. Kopple: Molecular properties that influence the oral bioavailability of drug candidates. *Journal of Medicinal Chemistry*, 45(12), 2615-2623 (2002)

56. J. A. Lessa, I. C. Mendes, P. R. O. da Silva, M. A. Soares, R. G. dos Santos, N. L. Speziali, N. C. Romeiro, E. J. Barreiro and H. Beraldo: 2-Acetylpyridine thiosemicarbazones: Cytotoxic activity in nanomolar doses against malignant gliomas. *European Journal of Medicinal Chemistry*, 45(12), 5671-5677 (2010) doi:DOI: 10.1016/j.ejmech.2010.09.021

57. X.-H. Liu, P.-Q. Chen, B.-L. Wang, Y.-H. Li, S.-H. Wang and Z.-M. Li: Synthesis, bioactivity, theoretical and molecular docking study of 1-cyano-N-substituted-cyclopropanecarboxamide as ketol-acid reductoisomerase inhibitor. *Bioorganic and Medicinal Chemistry Letters*, 17(13), 3784-3788 (2007) doi:DOI: 10.1016/j.bmcl.2007.04.003

58. E. C. M. Nascimento and J. B. L. Martins: Electronic structure and PCA analysis of covalent and non-covalent acetylcholinesterase inhibitors. *Journal of Molecular Modeling*, 17(6), 1371-1379 (2011)

59. A. Rayan: New tips for structure prediction by comparative modeling. *Bioinformation*, 3(6), 263-267 (2009)

60. R. A. Laskowski, M. W. MacArthur, D. S. Moss and J. M. Thornton: PROCHECK: a program to check the stereochemical quality of protein structures. *Journal of Applied Crystallography*, 26(2), 283-291 (1993) doi:doi:10.1107/S0021889892009944

61. P. Benkert, S. C. E. Tosatto and D. Schomburg: QMEAN: A comprehensive scoring function for model quality assessment. *Proteins: Structure, Function and Genetics*, 71(1), 261-277 (2008)

62. F. Melo and E. Feytmans: Assessing protein structures with a non-local atomic interaction energy. *Journal of Molecular Biology*, 277(5), 1141-1152 (1998)

63. P. Benkert, M. Biasini and T. Schwede: Toward the estimation of the absolute quality of individual protein structure models. *Bioinformatics*, 27(3), 343-350 (2011)

64. A. Achari, D. O. Somers, J. N. Champness, P. K. Bryant, J. Rosemond and D. K. Stammers: Crystal structure of the anti-bacterial sulfonamide drug target dihydropteroate synthase. *Nature Structural Biology*, 4(6), 490-497 (1997)

65. M. R. Sawaya and J. Kraut: Loop and subdomain movements in the mechanism of Escherichia coli dihydrofolate reductase: Crystallographic evidence. *Biochemistry*, 36(3), 586-603 (1997)

66. V. Cody and C. H. Schwalbe: Structural characteristics of antifolate dihydrofolate reductase enzyme interactions. *Crystallography Reviews*, 12(4), 301-333 (2006)

Key Words: Hybrid-drug Design, Multi-Target Inhibitors, Phytochemicals, Drug Resistance, Dihydrofolate Reductase, Dihydropteroate Synthase, Dual Action Compounds

Send correspondence to: Meena K. Sakharkar, School of Life and Environmental Sciences, University of Tsukuba, Tsukuba, Ibaraki, Japan, Tel- 81-29-853-8834, Fax: 81-29-853-4922, E-mail: msakharkar@gmail.com